Frontiers in Computing and Intelligent Systems
ISSN: 2832-6024 | Vol. 8, No. 1, 2024

Tracking Control Based on Model Predictive and Adaptive Neural Network Sliding Mode of Tiltrotor UAV

Zijing Ouyang, Sheng Xu and Chengyue Su

School of Physics and Optoelectronic Engineering, Guangdong University of Technology, Guangzhou Guangdong, 510006, China

Abstract: As the low-altitude economy rapidly expands, the demand for UAVs is increasingly growing, and their operational scenarios are becoming more complex, with higher requirements for endurance and short-distance take-off and landing performance. Tiltrotor UAVs, characterized by vertical take-off and landing and long endurance, have attracted widespread attention for their potential applications. However, the dynamics and flight paths of tiltrotor UAVs are highly nonlinear, and traditional linear flight controllers cannot fully utilize the real-time performance capabilities of tiltrotor UAVs. Under the conditions of model uncertainty and input saturation in tiltrotor UAVs, traditional LOS+PID control strategies exhibit characteristics of insufficient responsiveness and excessive overshoot. To improve the performance of tiltrotor UAVs in completing path tracking tasks, we have developed a new control strategy. By establishing an error model for three-dimensional space path tracking, we propose a cascaded control strategy of motion controllers and dynamic controllers. The motion controller is designed based on model predictive control, generating a series of speed-limited signals. Then, in the dynamic controller part, an adaptive radial basis function neural network is used to estimate the model uncertainty caused by aerodynamic parameters to enhance its robustness. Finally, the proposed algorithm is compared with the LOS guidance method and PID controller through simulation experiments. The comparison results show that the proposed algorithm can improve the path tracking effect, increase the response speed, and reduce the overshoot.

Keywords: Tiltrotor UAV; Model Predictive Control; Adaptive Neural Network Sliding Mode; Trajectory Tracking.

1. Introduction

It is well-known that the dynamics of tiltrotor UAVs are highly nonlinear, with strong coupling between longitudinal and lateral dynamics. Therefore, the control issues of tiltrotor UAVs present new challenges to control engineers.

However, with the rapid development of sensor technology, automatic control and microelectronics technology, energy supply, and communication technology in recent years, the design and manufacturing of tilt-rotor aircraft have achieved new breakthroughs. Many researchers have resumed the study of tiltrotor UAVs and have achieved many remarkable results.

In 2007, Hoffmann G M introduced a trajectory tracking control scheme based on error decomposition, which divided the trajectory error into tangential and normal components, compensated by PI and PID controllers respectively. This approach enabled path tracking and speed adjustment of unmanned aerial vehicles (UAVs), providing temporal flexibility in their tracking performance [1]. In 2008, Bouktir Y proposed a trajectory planning method based on B-spline equations, which utilized nonlinear optimization to derive time-optimal trajectories, albeit requiring significant computational resources [2]. Mellinger D, in 2011, put forward a PD-based trajectory tracking control scheme that employed PD controllers for feedback control of the UAV's position and attitude, achieving precise trajectory tracking [3]. As research progressed, Sliding Mode Control (SMC) algorithms, known for their low model dependency and excellent robustness, have been widely applied in the control of quadrotor UAVs. For instance, Mofid and colleagues studied the position controller for quadrotor UAVs and implemented attitude stabilization using the Terminal Sliding Mode Control (TSMC) algorithm [4].

Reference [5] proposed an Elevator Aileron (EA) control method based on Linear Quadratic Regulation (LQR) for the short-period approximation of the longitudinal model of tiltrotor unmanned aerial vehicles. However, stability remains a primary concern for linear control techniques, especially during operations at high pitch angles. The model's uncertainties were not considered due to the difficulty in accurately modeling tiltrotor UAVs. To ensure robustness against model uncertainties, numerous studies have focused on control theories such as gain scheduling [6], adaptive control [7-10], Sliding Mode Control (SMC) [11,12], and neural network control [13].

Taking into account the constraints on control deflection and rate, reference [14] introduced a Model Predictive Control (MPC) algorithm to address the issues of depth tracking and attitude control for tiltrotor unmanned aerial vehicles. However, both algorithms are based on nominal models.

Therefore, building on existing research, this paper integrates several algorithms including Model Predictive Control (MPC), Radial Basis Function Neural Network (RBFNN), and Adaptive Sliding Mode Control (ASMC). Chapter Two presents the kinematic and dynamic modeling of tiltrotor unmanned aerial vehicles. Chapter Three describes the error model, motion controller, and dynamic controller for tiltrotor UAVs. Simulation results are presented in Chapter Four, along with an evaluation of the overall performance of the controllers. Chapter Five concludes the paper.

2. Motion Modeling of Tiltrotor UAV

In this paper, the lift of the tiltrotor unmanned aerial vehicle is generated by the combined forces of the engine thrust, the aerodynamic force provided by the wings, and the gravity of the vehicle itself. The mass of the tiltrotor UAV is m_T=1.5kg. Due to the consideration of part universality in previous designs, the motors, electronic speed controllers, and propellers providing thrust to the tiltrotor UAV are of the same model as those used in the quadrotor UAV discussed in this paper. The fuselage is equipped with four motors symmetrically distributed on both sides of the tiltrotor UAV, with each motor positioned at a distance of d_T=600mm from the geometric center of the tiltrotor UAV, and the wing area being S_T=720000mm^2. Since the motors, electronic speed controllers, and propellers of the same model as those used in the quadrotor UAV are employed, the rotational radius of the propeller blades r, the propeller thrust coefficient, and the propeller torque coefficient cm are universal to the quadrotor UAV discussed in this paper. The rotational speeds of the four motors of the tiltrotor UAV are w_{T1}, w_{T2}, w_{T3}, and w_{T4}, respectively, with the tilt angles of motor 1 and motor 4 being adjustable and identical at angle α. To counteract the torque effect during flight, one pair of diagonally opposite motors rotates clockwise, while the other pair rotates counterclockwise, generating a reactive force through the rotation of the rotors on the motors, thereby providing power output.

The body coordinate system for the tiltrotor unmanned aerial vehicle is designated as {T}. The origin ^TO_T of the tiltrotor UAV's body coordinate system {T} is situated at the center of the UAV's fuselage, with the positive direction of the x-axis aligned with the UAV's forward direction, the z-axis perpendicular to the fuselage's belly plane and pointing downward, and the y-axis perpendicular to both the x-axis and z-axis, pointing to the right side of the quadrotor UAV's forward direction. The coordinate system {G} is defined as the terrestrial coordinate system. To facilitate calculations, the UAV's initial position is set as the origin ^GO_G of the terrestrial coordinate system {G}, with the x-axis of {G} being horizontal to the ground and pointing east, the y-axis horizontal to the ground and pointing south, and the z-axis perpendicular to the ground.

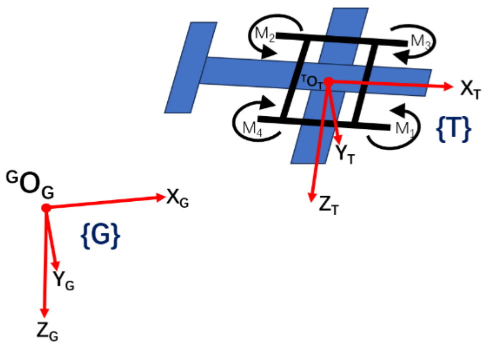

Fig 1. Definition of various coordinate systems.

Consequently, the kinematic and dynamic models for the underactuated tiltrotor unmanned aerial vehicle are as follows:

$$\dot{\eta}_T = J_T v_T \tag{1}$$

$$\Omega_T \dot{v}_T + \Phi_T v_T + \Upsilon_T = f_T + b_T \tag{2}$$

Within this context, $\eta_T = [{}^G x_T \;\; {}^G y_T \;\; {}^G z_T \;\; \phi_T \;\; \vartheta_T \;\; \psi_T]^T$ is the position and orientation of the tiltrotor unmanned aerial vehicle within the {G} coordinate frame. The terms (${}^G x_T \;\; {}^G y_T \;\; {}^G z_T$) and ($\phi_T \;\; \vartheta_T \;\; \psi_T$) correspond to the position and orientation in the {G} frame, respectively. $v_T = [u_T \;\; v_T \;\; w_T \;\; p_T \;\; q_T \;\; r_T]^T$ is the vectors of translational velocity and angular velocity in the {T} frame. The velocities u, v, w along the x, y, and z axes of the {T} frame, respectively, and the angular velocities p, q, r represents the roll, pitch, and yaw rates in the {T} frame. The matrix J_T represents the rotational transformation from the {T} to the {G} frame:

$$J_T = \begin{bmatrix} {}^G_T R & 0_{3\times3} \\ 0_{3\times3} & {}^G_T W \end{bmatrix} \tag{3}$$

In this matrix, the forms of matrices ${}^G_T R$ and ${}^G_T W$ are as follows:

$${}^G_T R = \begin{bmatrix} \cos\vartheta_T \cos\psi_T & \cos\psi_T \sin\vartheta_T \sin\phi_T - \cos\phi_T \sin\psi_T & \sin\phi_T \sin\psi_T + \cos\phi_T \cos\psi_T \sin\vartheta_T \\ \cos\vartheta_T \sin\psi_T & \cos\phi_T \cos\psi_T + \sin\vartheta_T \sin\phi_T \sin\psi_T & \cos\phi_T \cos\vartheta_T \sin\psi_T - \cos\psi_T \sin\psi_T \\ -\sin\vartheta_T & \cos\vartheta_T \sin\phi_T & \cos\vartheta_T \cos\phi_T \end{bmatrix} \tag{4}$$

$${}^G_T W = \begin{bmatrix} 1 & \sin\phi_T \tan\vartheta_T & \cos\vartheta_T \sin\phi_T \\ 0 & \cos\phi_T & -\sin\phi_T \\ 0 & \sin\vartheta_T / \cos\vartheta_T & \cos\phi_T / \cos\vartheta_T \end{bmatrix} \tag{5}$$

The matrices Ω_T, Φ_T, Υ_T are as follows:

$$\Omega_T = \begin{bmatrix} m_T & \\ & I_T \end{bmatrix}, I_T = \begin{bmatrix} I_{Txx} & & \\ & I_{Tyy} & \\ & & I_{Tzz} \end{bmatrix}, \Phi_T = \frac{1}{2}\rho S_T \begin{bmatrix} C_x & & & & & \\ & C_y & & & & \\ & & C_z & & & \\ & & & C_l & & \\ & & & & C_m & \\ & & & & & C_n \end{bmatrix}, \Upsilon_T = \begin{bmatrix} {}^G_T R^T \begin{bmatrix} 0 \\ 0 \\ m_T g \end{bmatrix} \\ 0_{3\times1} \end{bmatrix} \tag{6}$$

The f_T is the control vector:

$$
f_T = \begin{bmatrix} c_t\left(w_{T1}^2+w_{T4}^2\right)\sin\alpha \\ 0 \\ -c_t\left(\left(w_{T1}^2+w_{T4}^2\right)\cos\alpha+w_{T2}^2+w_{T3}^2\right) \\ c_t\left(\left(-w_{T1}^2+w_{T3}^2\right)\cos\alpha+w_{T2}^2-w_{T4}^2\right)d_T+c_m\left(w_{T1}^2-w_{T3}^2\right)\sin\alpha \\ c_t\left(\left(w_{T1}^2+w_{T3}^2\right)\cos\alpha-w_{T2}^2-w_{T4}^2\right)d_T \\ c_t d_T\left(-w_{T1}^2+w_{T2}^2\right)\sin\alpha+c_m\left(\left(-w_{T1}^2 w_{T4}^2+w_{T3}^2\right)\cos\alpha-w_{T2}^2+w_{T4}^2\right) \end{bmatrix} \tag{7}
$$

In this vector, the c_t and c_m denote the thrust coefficient and torque coefficient of the motor.

The vector b_T describes the uncertainty of tiltrotor UAV model.

3. Design of a Tilt-Wing UAV Controller based on Model Predictive Control and Adaptive Sliding Mode Control

References In this chapter, we will employ two methodologies, Model Predictive Control (MPC) and Adaptive Sliding Mode Control (ASMC), for the design of controllers for tiltrotor UAV. Initially, a model based on flight path tracking error will be constructed. Subsequently, a kinematic controller utilizing MPC will be designed, along with a dynamic controller based on ASMC. To address uncertainties arising from modeling precision, this section will integrate Radial Basis Function (RBF) neural networks into the sliding mode control to estimate such uncertainties. Following this, we will simulate the flight performance of the tiltrotor UAVs using these controllers and conduct tests on waypoint tracking, straight-line path tracking, spiral path tracking, and wave path tracking. The objective of this chapter is to explore and understand how to formulate efficient and stable control strategies that enable precise execution of various types of flight maneuvers by tiltrotor UAVs through the application of MPC and ASMC methods.

3.1. Design of Kinematic Controllers for Tiltrotor UAV Based on Model Predictive Control

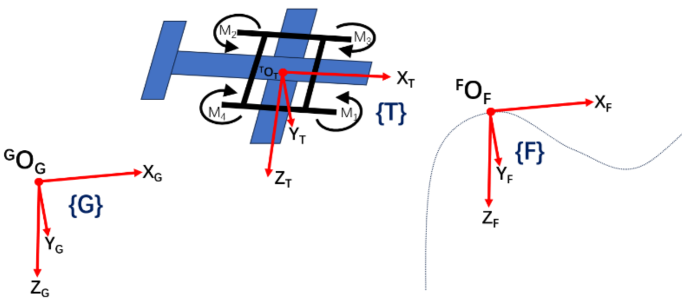

Fig 2. Establishing the Frenet coordinate system.

To track the desired trajectory, a Frenet frame {F} is established at the current point on the traced path. The directions of the unit tangent vector, unit normal vector, and unit binormal vector at the current point on the traced path are defined as the x, y, and z axis directions of the Frenet frame {F}, respectively. This coordinate system is used to develop a three-dimensional tracking error model. The origin P of the Frenet frame {F} is treated as a virtual target moving along the expected path, which the unmanned aerial vehicle (UAV) tracks. A controller is designed to stabilize the error to zero, as depicted in Figure 2.

Referring to Figure 3-1, let s be defined as the distance traveled by point P along the traced path, c_c as the curvature, and c_t as the torsion. Then, the pitch rate and yaw rate of the Frenet frame {F} can be calculated according to the following equations:

$$
q_F = c_t\dot{s} = c_t u_F,\ r_F = c_c\dot{s} = c_c u_F,\ \dot{s} = u_F \tag{8}
$$

These equations facilitate the determination of the dynamic behavior of the UAV in relation to the desired path, enabling precise control strategies for trajectory tracking.

The path tracking task can be transformed into the stability problem of the following system:

$$
\begin{bmatrix} \dot{x}_e \\ \dot{y}_e \\ \dot{z}_e \\ \dot{\phi}_e \\ \dot{\theta}_e \\ \dot{\psi}_e \\ \dot{p}_e \\ \dot{q}_e \\ \dot{r}_e \end{bmatrix} = \begin{bmatrix} u\cos\theta_e + uk_x\psi_e - \left(u_{ed}+u_d\right) - q_F z_e + r_F y_e + d_x \\ uk_y\psi_e - r_F x_e + d_y \\ -uk_z\theta_e + q_F x_e + d_z \\ p_e \\ q_e \\ -q_F\psi_e\tan\theta_F + \dfrac{\left(r_e+r_F\right)\cos\theta_F}{\cos\theta} - r_F \\ \left(p-p_d\right)/T_1 \\ \left(q_{ed}-q_e\right)/T_2 - \dot{q}_F \\ \left(r_{ed}-r_e\right)/T_3 - \dot{r}_F \end{bmatrix} \tag{9}
$$

And $k_x = \cos\theta_e(\cos\psi_e - 1)/\psi_e$, $k_y = \cos\theta_e\sin\psi_e/\psi_e, k_z = \sin\theta_e/\theta_e$.

Therefore, the control system (9) can be considered as:

$$
\dot{\boldsymbol{x}} = f(\boldsymbol{x}, \boldsymbol{u}) \tag{10}
$$

In this context, $\boldsymbol{x} = [x_e\ y_e\ z_e\ \phi_e\ \vartheta_e\ \psi_e\ p_e\ q_e\ r_e]^T$ represents the state variables, while $\boldsymbol{u} = [u_{ed}\ q_{ed}\ r_{ed}]^T$ denotes the input variables. $\boldsymbol{x} = [x_e\ y_e\ z_e\ \phi_e\ \vartheta_e\ \psi_e\ p_e\ q_e\ r_e]^T$ constitutes an augmented error matrix comprising errors in position, orientation, and angular velocity. s At the equilibrium point, the control system given by equation (10) can be discretized as follows:

$$
\boldsymbol{x}(k+1) = \boldsymbol{A}_k\boldsymbol{x}(k) + \boldsymbol{B}_k\boldsymbol{u}(k) \tag{11}
$$

In the context of discretization, matrices $\boldsymbol{A}_k$ and $\boldsymbol{B}_k$ correspond to the system matrix and the control input matrix of the state equation, respectively. Their specific forms are presented as:

$$
\boldsymbol{A_k}=\begin{bmatrix}
1 & Tr_F & -Tq_F & 0 & 0 & A_k^{16} & 0 & 0 & 0\\
-Tr_F & 1 & 0 & 0 & 0 & A_k^{26} & 0 & 0 & 0\\
Tq_F & 0 & 1 & 0 & A_k^{35} & 0 & 0 & 0 & 0\\
0 & 0 & 0 & 0 & 0 & 0 & 0 & 0 & 0\\
0 & 0 & 0 & 0 & 1 & 0 & 0 & T & 0\\
0 & 0 & 0 & 0 & 0 & A_k^{66} & 0 & 0 & A_k^{69}\\
0 & 0 & 0 & 0 & 0 & 0 & 0 & 0 & 0\\
0 & 0 & 0 & 0 & 0 & 0 & 0 & 1-T/T_1 & 0\\
0 & 0 & 0 & 0 & 0 & 0 & 0 & 0 & 1-T/T_2
\end{bmatrix},
$$

$$
\boldsymbol{B_k}=\begin{bmatrix}
-T & 0 & 0\\
0 & 0 & 0\\
0 & 0 & 0\\
0 & 0 & 0\\
0 & 0 & 0\\
0 & 0 & 0\\
0 & 0 & 0\\
0 & T/T_1 & 0\\
0 & 0 & T/T_2
\end{bmatrix},\quad
\begin{bmatrix} A_k^{16}\\ A_k^{26}\\ A_k^{35}\\ A_k^{66}\\ A_k^{69}\end{bmatrix}=\begin{bmatrix} Tuk_x\\ Tuk_y\\ -Tuk_z\\ 1-Tq_F\tan\theta_F\\ \mathrm{T}\cos\theta_F/\cos\theta\end{bmatrix} \tag{12}
$$

Within the model predictive control framework, where only new state variables are reselected, the state quantity $\bar{\boldsymbol{x}}(k)$ is defined as:

$$
\bar{\boldsymbol{x}}(k)=\begin{bmatrix}\boldsymbol{x}(k)\\ \boldsymbol{u}(k-1)\end{bmatrix} \tag{13}
$$

Consequently, future state variables can be expressed as:

$$
\begin{aligned}
\bar{\boldsymbol{x}}(k+1)&=\bar{\boldsymbol{A}}_k\bar{\boldsymbol{x}}(k)+\boldsymbol{B}_k\Delta\boldsymbol{u}(k),\\
\bar{\boldsymbol{x}}(k+2)&=\bar{\boldsymbol{A}}_k\bar{\boldsymbol{x}}(k+1)+\boldsymbol{B}_k\Delta\boldsymbol{u}(k+1)\\
&=\bar{\boldsymbol{A}}_k^2\bar{\boldsymbol{x}}(k)+\boldsymbol{A}_k\bar{\boldsymbol{B}}_k\Delta\boldsymbol{u}(k)+\boldsymbol{B}_k\Delta\boldsymbol{u}(k+1),\\
&\ \,\vdots\\
\bar{\boldsymbol{x}}\left(k+N_p\right)&=\bar{\boldsymbol{A}}_k^{N_p}\bar{\boldsymbol{x}}(k)+\boldsymbol{A}_k^{N_p-1}\bar{\boldsymbol{B}}_k\Delta\boldsymbol{u}(k)\\
&\quad+\cdots+\bar{\boldsymbol{A}}_k^{N_p-N_c}\bar{\boldsymbol{B}}_k\Delta\boldsymbol{u}\left(k+N_c-1\right),
\end{aligned} \tag{14}
$$

In this context, it is stipulated that $N_c<N_p$. Herein, N_p denotes the prediction horizon, while N_c signifies the control horizon. In (14), the explicit forms of parameters $\bar{\boldsymbol{A}}_k$, $\bar{\boldsymbol{B}}_k$, $\Delta\boldsymbol{u}(k)$, and $\bar{\boldsymbol{C}}_k$ are detailed as follows:

$$
\bar{\boldsymbol{A}}_k=\begin{bmatrix}\boldsymbol{A}_k & \boldsymbol{B}_k\\ 0_{3\times9} & \mathbf{I}_3\end{bmatrix},\ \bar{\boldsymbol{B}}_k=\begin{bmatrix}\boldsymbol{B}_k\\ \mathbf{I}_3\end{bmatrix},
$$

$$
\Delta\boldsymbol{u}(k)=\boldsymbol{u}(k)-\boldsymbol{u}(k-1)\,,\bar{\boldsymbol{C}}_k=\begin{bmatrix}\mathbf{I}_3 & \mathbf{0}_{3\times9}\end{bmatrix} \tag{15}
$$

Consequently, the future output variable can be predicted as:

$$
\begin{aligned}
\boldsymbol{y}(k+1)&=\bar{\boldsymbol{C}}_k\bar{\boldsymbol{A}}_k\bar{\boldsymbol{x}}(k)+\boldsymbol{C}_k\bar{\boldsymbol{B}}_k\Delta\boldsymbol{u}(k),\\
\boldsymbol{y}(k+2)&=\bar{\boldsymbol{C}}_k\bar{\boldsymbol{A}}_k^2\bar{\boldsymbol{x}}(k)+\boldsymbol{C}_k\bar{\boldsymbol{A}}_k\bar{\boldsymbol{B}}_k\Delta\boldsymbol{u}(k)+\boldsymbol{C}_k\bar{\boldsymbol{B}}_k\Delta\boldsymbol{u}(k+1),\\
&\ \,\vdots\\
\boldsymbol{y}\left(k+N_p\right)&=\bar{\boldsymbol{C}}_k\bar{\boldsymbol{A}}_k^{N_p}\bar{\boldsymbol{x}}(k)+\boldsymbol{C}_k\bar{\boldsymbol{A}}_k^{N_p-1}\bar{\boldsymbol{B}}_k\Delta\boldsymbol{u}(k)\\
&\quad+\cdots+\bar{\boldsymbol{C}}_k\bar{\boldsymbol{A}}_k^{N_p-N_c}\bar{\boldsymbol{B}}_k\Delta\boldsymbol{u}\left(k+N_c-1\right).
\end{aligned} \tag{16}
$$

The following results were obtained upon consolidation:

$$
\boldsymbol{Y(k+1)=Mx(k)+P\Delta U(k)} \tag{17}
$$

$$
\boldsymbol{Y}(k+1)=\begin{bmatrix}\boldsymbol{y}(k+1)\\ \boldsymbol{y}(k+2)\\ \boldsymbol{y}(k+3)\\ \vdots\\ \boldsymbol{y}\left(k+N_p\right)\end{bmatrix},\boldsymbol{M}=\begin{bmatrix}\bar{\boldsymbol{C}}_k\bar{\boldsymbol{A}}_k\\ \bar{\boldsymbol{C}}_k\bar{\boldsymbol{A}}_k^2\\ \bar{\boldsymbol{C}}_k\bar{\boldsymbol{A}}_k^3\\ \vdots\\ \bar{\boldsymbol{C}}_k\bar{\boldsymbol{A}}_k^{N_p}\end{bmatrix},\boldsymbol{P}=\begin{bmatrix}
\bar{\boldsymbol{C}}_k\bar{\boldsymbol{B}}_k & \boldsymbol{0} & \boldsymbol{0} & \cdots & \boldsymbol{0}\\
\bar{\boldsymbol{C}}_k\bar{\boldsymbol{A}}_k\bar{\boldsymbol{B}}_k & \bar{\boldsymbol{C}}_k\bar{\boldsymbol{B}}_k & \boldsymbol{0} & \cdots & \boldsymbol{0}\\
\bar{\boldsymbol{C}}_k\bar{\boldsymbol{A}}_k^2\bar{\boldsymbol{B}}_k & \bar{\boldsymbol{C}}_k\bar{\boldsymbol{A}}_k\bar{\boldsymbol{B}}_k & \bar{\boldsymbol{C}}_k\bar{\boldsymbol{B}}_k & \cdots & \boldsymbol{0}\\
\vdots & \vdots & \vdots & \ddots & \vdots\\
\bar{\boldsymbol{C}}_k\bar{\boldsymbol{A}}_k^{N_p\text{-}1}\bar{\boldsymbol{B}}_k & \bar{\boldsymbol{C}}_k\bar{\boldsymbol{A}}_k^{N_p\text{-}2}\bar{\boldsymbol{B}}_k & \bar{\boldsymbol{C}}_k\bar{\boldsymbol{A}}_k^{N_p\text{-}3}\bar{\boldsymbol{B}}_k & \cdots & \bar{\boldsymbol{C}}_k\bar{\boldsymbol{A}}_k^{N_p\text{-}N_c}\bar{\boldsymbol{B}}_k
\end{bmatrix} \tag{18}
$$

In this study, the parameters $\Delta\boldsymbol{u}_{\min}$ and $\Delta\boldsymbol{u}_{\max}$ are defined as the minimum and maximum variations in input quantity, respectively, while $\boldsymbol{u}_{\min}$ and $\boldsymbol{u}_{\max}$ represent the minimum and maximum values of the input quantity. Control variable amplitude and increment constraints are taken into account as follows:

$$
\begin{cases}\Delta\boldsymbol{u}_{\min}\le\Delta\boldsymbol{u}(t+k)\le\Delta\boldsymbol{u}_{\max}\,,k=0,1,\cdots N_c-1\\ \boldsymbol{u}_{\min}\le\boldsymbol{u}(t+k)\le\boldsymbol{u}_{\max}\,,k=0,1,\cdots N_c-1\end{cases} \tag{19}
$$

Regarding the stability issue of the system, it is imperative to ensure that the predicted output remains as close to zero as possible within the forecasting horizon. The task of the Model Predictive Controller is to compute the optimal control vector $\Delta\boldsymbol{U}$, which minimizes the predicted output. The cost function J_{cost}, chosen as the sum of terminal and input costs, is formulated as:

$$
\mathrm{J}_{\text{cost}}=\boldsymbol{Y}(k+1)^T\boldsymbol{QY}(k+1)+\Delta\boldsymbol{U}(k)^T\boldsymbol{R}\Delta\boldsymbol{U}(k) \tag{20}
$$

Wherein $\boldsymbol{Q}$ and $\boldsymbol{R}$ denote:

$$
\boldsymbol{Q}=\mathbf{I}_{N\rho}\otimes\begin{bmatrix}Q_1 &&&&&&\\ & Q_2 &&&&&\\ && Q_3 &&&&\\ &&& Q_4 &&&\\ &&&& Q_5 &&\\ &&&&& Q_6 &\\ &&&&&& Q_7\end{bmatrix},
$$

$$
\boldsymbol{R}=\mathbf{I}_{Nc}\otimes\begin{bmatrix}R_1 &&\\ & R_2 &\\ && R_3\end{bmatrix} \tag{21}
$$

Taking into account the constraints at each step, the optimization problem of MPC can be equivalently addressed through the solution of the subsequent quadratic programming:

$$\min_{\Delta U} J_{\text{cost}} = \boldsymbol{Y}(k+1)^T \boldsymbol{QY}(k+1) + \Delta \boldsymbol{U}(k)^T \boldsymbol{R} \Delta \boldsymbol{U}(k) \tag{22}$$

Upon entering the next sampling period, the MPC will reiterate the aforementioned process and recalculate the control signal based on the most recently measured state vector.

3.2. Design of Dynamic Controllers for Tiltrotor UAV Based on Radial Basis Function Neural Network Adaptive Sliding Mode Control

This section will present the development of a dynamic controller. The error variable and the sliding mode function are defined as:

$$z_1 = v_d - v_a, z_2 = \int_0^t z_1 \mathrm{d}\tau, s = z_1 + \mathrm{k}_s z_2 + u_{aux}, u_{aux} = than(z_1)$$

,

$$v_d = [u_d q_d r_d]^{\mathrm{T}}, \mathrm{k}_s = \mathrm{diag}(\mathrm{k}_{s1}\ \mathrm{k}_{s2}\ \mathrm{k}_{s3}) \geq 0 \tag{23}$$

For the nonlinear uncertainty $\mathrm{b_T}$ in the dynamics model of a tiltrotor UAV, an approximation using radial basis function neural networks is employed in the following manner:

$$\mathrm{b_T} = W^{*T}\mathbf{h}(\mathbf{x}_{\text{in}}) + \boldsymbol{\varepsilon}, x_{\text{in}} = [v_{\mathrm{T}}^T z_l^T]^T,$$

$$h_i(\mathbf{x}_{\text{in}}) = \exp\Big(-\frac{\| \mathbf{x}_{in} - \mathbf{c}_i \|^2}{2b_i^2}\Big), \quad i = 1,2,3\ldots \tag{24}$$

And the $\boldsymbol{\varepsilon}$ is the estimation error. The output of the radial basis function neural network is defined as $\hat{\mathrm{b}}_{\mathrm{T}} = \widehat{W}^{\mathrm{T}} h(x_{\text{in}})$. Matrix $\widehat{W}^{\mathrm{T}}$ represents the estimation of optimal weights, while $\tilde{W} = W^* - \hat{W}$ denotes the estimation error.

Therefore, the control law for the kinematic controller of tiltrotor UAV can be designed as:

$$\begin{cases} \mathrm{f_T} = \Omega_{\mathrm{T}}\dot{\mathrm{v}}_{\mathrm{T}} + \Phi_{\mathrm{T}}\mathrm{v}_{\mathrm{T}} + \Upsilon_{\mathrm{T}} - \hat{\mathrm{b}}_{\mathrm{T}} + \Omega_{\mathrm{T}} k_s \dot{e} + K_1 s + K_2 sgn(s) \\ W = -h(x_{in}) s^T / \gamma \end{cases} \tag{25}$$

And $K_1 = \mathrm{diag}(k_{11}, k_{12}, k_{13}) \geq 0$, $K_2 = \mathrm{diag}(k_{21}, k_{22}, k_{23}) \geq 0$, $k_{2i} = k_{\varepsilon 1}(1 - e^{-k_\varepsilon |s_i|})$, $k_{\varepsilon 1} > 0$, $k_{\varepsilon 2} > 0$, (i=1, 2, 3)

To validate the stability of the system with the added controller, we may select a Lyapunov function as follows:

$$V = s^{\mathrm{T}}\Omega_{\mathrm{T}} s / 2 + \gamma \mathrm{tr}(\tilde{W}^{\mathrm{T}}\tilde{W}) / 2 \tag{26}$$

In this context, γ represents a constant, and it must satisfy the condition $\gamma > 0$. Given that all terms within the function are positive, it follows that $V > 0$.

Differentiating the Lyapunov function V with respect to time yields:

$$\dot{V} = s^{\mathrm{T}}\mathbf{M}_a \dot{s} - \gamma \mathrm{tr}\big(\widetilde{\mathbf{W}}^{\mathrm{T}} \dot{\widehat{\mathbf{W}}}\big) \tag{27}$$

Since each term in formula (dd) is non-negative, it follows that $\dot{V} < 0$. Therefore, it is affirmed that the application of the controller results in the aileron dynamics system being progressively stable.

4. Simulation Experiment

This section will introduce the simulation results of the kinematic controller based on Model Predictive Control and the dynamic controller based on Sliding Mode Control in MATLAB.

4.1. Simulation Program Development

The control framework for the tiltrotor UAV is shown in Figure:

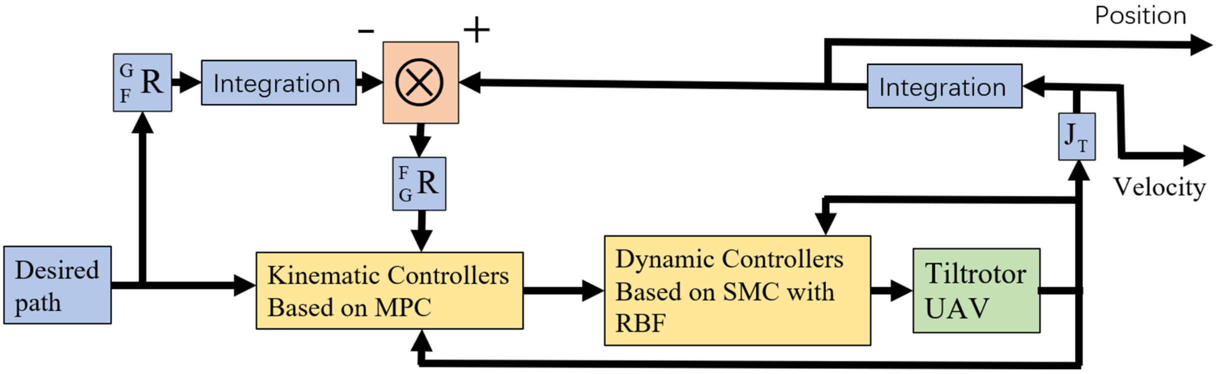

Fig 3. The control framework for the tiltrotor UAV

To validate the control effectiveness of the kinematic controller based on Model Predictive Control (MPC) and the dynamic controller based on Radial Basis Function (RBF) Neural Network adaptive sliding mode control for tiltrotor UAV, it is necessary to conduct simulation experiments on MATLAB to demonstrate the efficacy of the final control strategy.

In the simulation experiments, the initial values for the position, attitude, velocity, angular velocity, acceleration, and angular acceleration of the tiltrotor UAV were set to zero. The simulation time for each path was 100 seconds. Under these conditions, the body coordinate system {T} of the tilt-wing UAV coincided with the Earth coordinate system {G}. The radial basis function neural network within the dynamics controller of the tilt-wing UAV consisted of 5 nodes. The centers c were located at [0 1.5], [-0.2 0.2], [-0.2 0.2], [-0.5 1], [-0.2 0.2], and [-0.2 0.2], respectively, with a width bi of 0.1 and a coefficient c of 0.5. The other design parameters of the controller are presented in Table 1.

Table 1. Parameters of the controller

$T_2 = 0.6$	$\Delta u_{max} = [0.2, 0.04, 0.04]$	$u_{max} = [1, 0.2, 0.2]$	$N_p = 10$	$N_c = 3$	$Q_7 = 1$
$T_1 = 0.6$	$\Delta u_{min} = [-0.2, -0.04, -0.04]$	$u_{min} = [-1, -0.2, -0.2]$	$Q_1 = 1$	$Q_2 = 1$	$R_1 = 1$
$T = 0.1$	$Q_6 = 1$	$Q_5 = 2$	$Q_4 = 3$	$Q_3 = 1$	$R_2 = 1$
$R_3 = 1$					

Additionally, the control performance of the proposed controller is compared with that of a Line-of-Sight (LOS)+Proportional-Integral-Derivative (PID) controller. The specific configuration of the LOS+PID controller is as follows:

$$\begin{cases} u_F = u\cos\psi_\theta \cos\theta_\theta + 0.1x_\theta, \\ \theta_{ed} = \tan^{-1}\left(\dfrac{z_e}{\Delta_\theta}\right), \\ \psi_{ed} = -\tan^{-1}\left(\dfrac{y_e}{\Delta_\psi}\right), \\ n_p = 20(u-u_d) + 7\int_0^t (u-u_d)d\tau + 6\dot{u}, \\ \delta_s = 3.5(\theta_e - \theta_{ed}) + 2.5\int_0^t (\theta_{ed} - \theta_{ed})d\tau + 4(\dot{\theta}_e - \dot{\theta}_{ed}), \\ \delta_r = 3.5(\psi_e - \psi_{ed}) + 2.5\int_0^t (\psi_e - \psi_{ed})d\tau + 4(\dot{\psi}_e - \dot{\psi}_{ed}), \end{cases} \tag{28}$$

4.2. Straight Line Path Tracking

The purpose of this simulation is to test the fundamental performance of the designed controller and to verify whether the controller can accurately track a basic straight reference path.

The reference path for the straight-line path tracking simulation experiment is:

$$\begin{bmatrix} x_d \\ y_d \\ z_d \end{bmatrix} = \begin{bmatrix} 15t + 120 \\ 15t + 120 \\ -100 \end{bmatrix} \tag{29}$$

Through the execution of simulation experiment, this study has successfully gathered performance data pertaining to the trajectory tracking task of tilt-rotor unmanned aerial vehicles.

The positional changes of the tiltrotor UAV during the trajectory tracking task in the geodetic coordinate system {G} are illustrated in the figure:

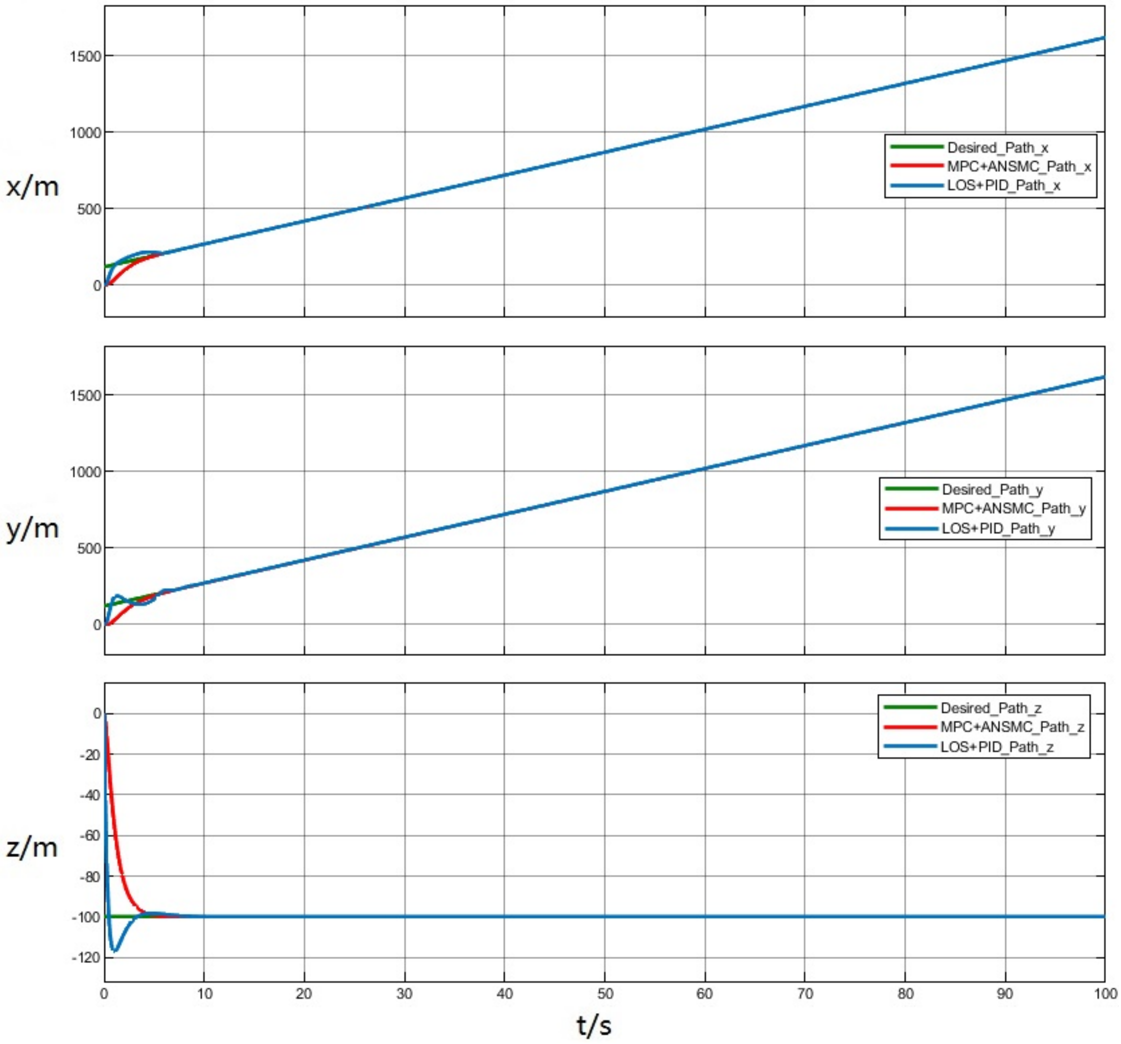

Fig 4. The positional variations of the tiltrotor UAV

In the figure, the green curve represents the input target trajectory, which is defined within the geodetic coordinate system {G}. The red curve illustrates the actual positional changes of the tiltrotor UAV while performing a trajectory tracking task under the controller designed in this study. The blue curve depicts the positional changes of the tiltrotor UAV executing the trajectory tracking task under a controller based on the Line-Of-Sight (LOS) plus Proportional-Integral-Derivative (PID) control strategy. It is observable that the time taken for the tiltrotor UAV to reach the position on the target trajectory at the current moment using the controller proposed in this paper is similar to that when employing the traditional LOS+PID controller. However, the overshoot is greater when the traditional LOS+PID controller is utilized.

The velocity variations of the tiltrotor UAV during the trajectory tracking task within the geodetic coordinate system {G} are depicted in the figure:

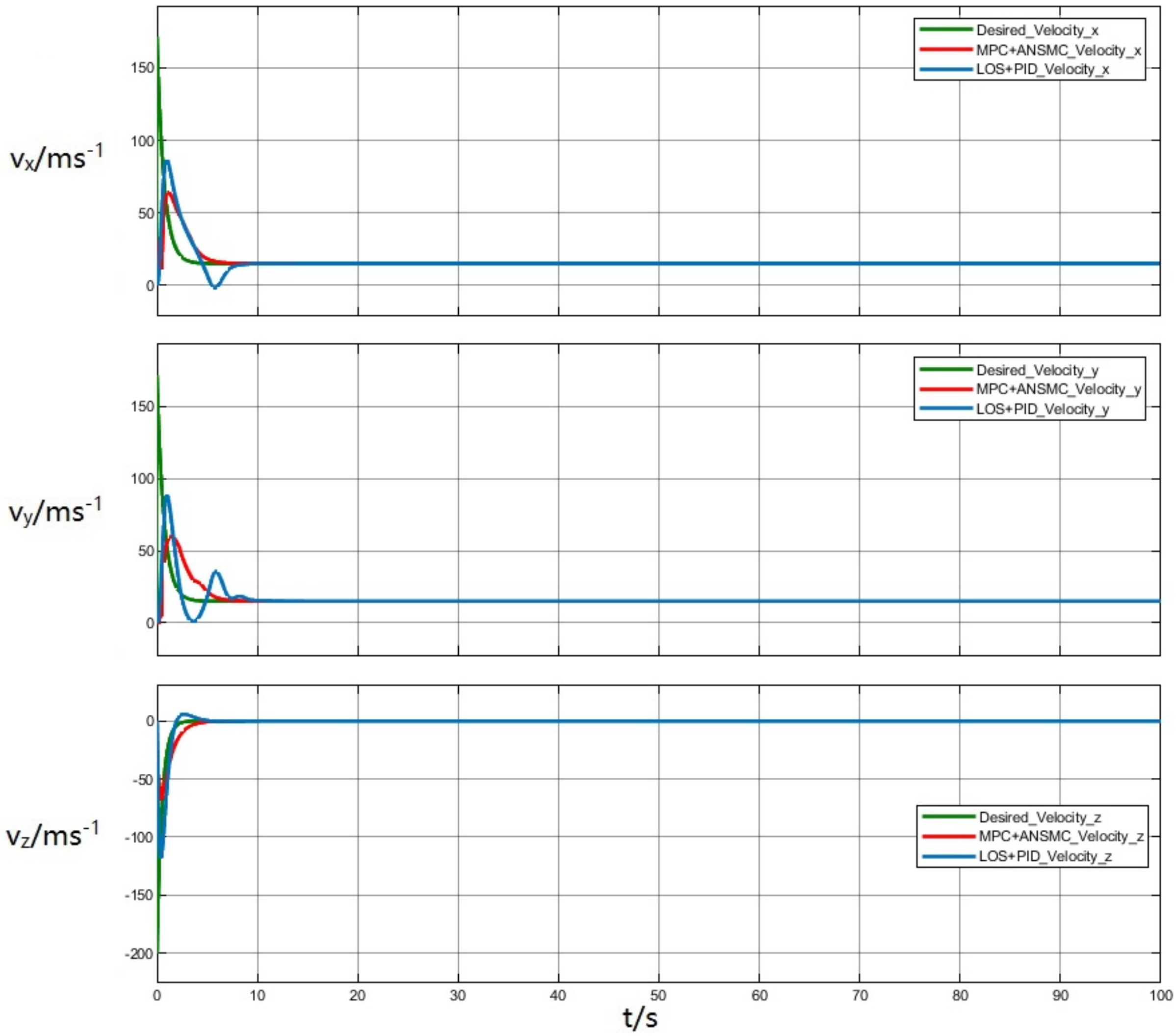

Fig 5. The velocity variations of the tiltrotor UAV

In the figure, the green curve represents the reference velocity obtained by processing the input target trajectory, which is coordinated within the geodetic coordinate system {G}. The red curve in the figure indicates the actual velocity variations of the tilt-rotor unmanned aerial vehicle when executing the trajectory tracking task under the controller designed in this paper. The blue curve represents the actual velocity variations of the tiltrotor UAV when executing the trajectory tracking task under a controller with a Line of Sight (LOS) plus Proportional-Integral-Derivative (PID) control strategy. It can be observed that compared to the traditional LOS+PID controller, the controller designed in this paper enables the tiltrotor UAV to accelerate to the target velocity more rapidly while maintaining smoother movements.

Variations in the magnitude of position errors for tilt-rotor unmanned aerial vehicles during trajectory tracking tasks within the geodetic coordinate system {G}:

In the figure, the red curve illustrates the error between the actual path and the target trajectory of the tilt-rotor unmanned aerial vehicle when executing the trajectory tracking task with the controller designed in this paper. The blue curve shows the error between the actual path and the target trajectory when the tilt-rotor unmanned aerial vehicle is using a controller with a LOS (Line of Sight) + PID (Proportional-Integral-Derivative) control strategy for the trajectory tracking task. It can be observed that both the traditional LOS+PID controller and the controller designed in this paper can enable the tilt-rotor unmanned aerial vehicle to quickly converge the error with the target trajectory. However, the controller designed in this paper allows the unmanned aerial vehicle to complete the task with less energy consumption.

The simulation results presented above indicate that, in the task of straight-line path tracking, the controller designed in this study demonstrates advantages of faster response and quicker convergence rates when compared to controllers employing a LOS+PID control strategy. Consequently, it can be inferred that it exhibits superior performance in tracking basic straight-line reference paths.

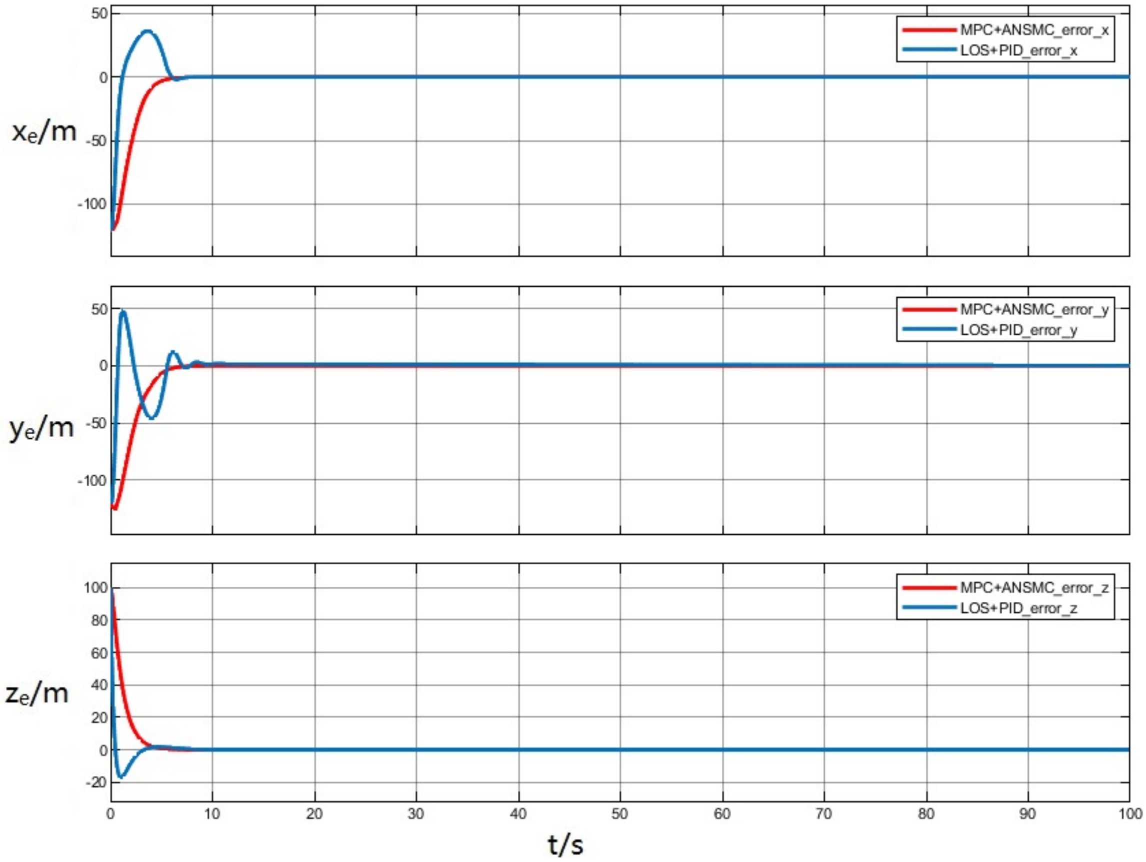

Fig 6. The positional errors of the tiltrotor UAV

4.3. Helical Curve Path Tracking

This segment of the simulation is designed to examine the actual performance of the developed controller and to verify its capability to effectively track common curved reference paths within a three-dimensional space.

The reference path for the helical curve path tracking simulation experiment is as follows:

$$\begin{bmatrix} x_d \\ y_d \\ z_d \end{bmatrix} = \begin{bmatrix} 25sin(0.6\pi t)+30 \\ 25cos(0.6\pi t)+30 \\ -12t-100 \end{bmatrix} \tag{30}$$

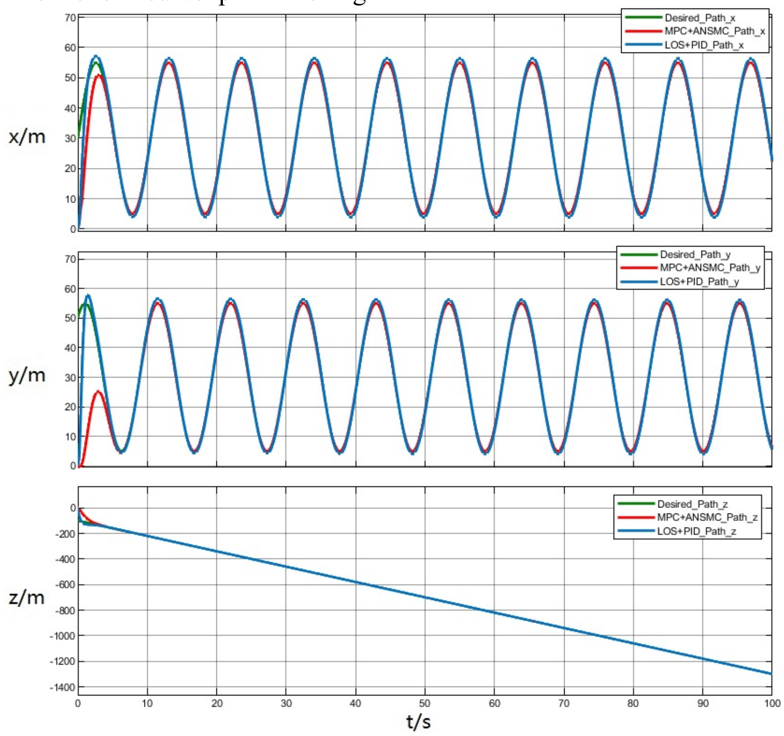

Fig 7. The positional variations of the tiltrotor UAV

Through the execution of simulation experiment, this study has successfully gathered performance data pertaining to the trajectory tracking task of tilt-rotor unmanned aerial vehicles.

The positional changes of the tiltrotor UAV during the trajectory tracking task in the geodetic coordinate system {G} are illustrated in the figure 7.

In the figure, the green curve represents the input target trajectory, which is defined in the geodetic coordinate system {G}. The red curve illustrates the actual position changes of the tiltrotor UAV when performing the trajectory tracking task under the controller designed in this paper. The blue curve shows the position changes of the tiltrotor UAV when executing the trajectory tracking task under a controller with a LOS+PID control strategy. It is evident that the tiltrotor UAV reaches the current target position on the trajectory more smoothly with the controller designed in this paper compared to the traditional LOS+PID controller.

The velocity variations of the tiltrotor UAV during the trajectory tracking task within the geodetic coordinate system {G} are depicted in the figure:

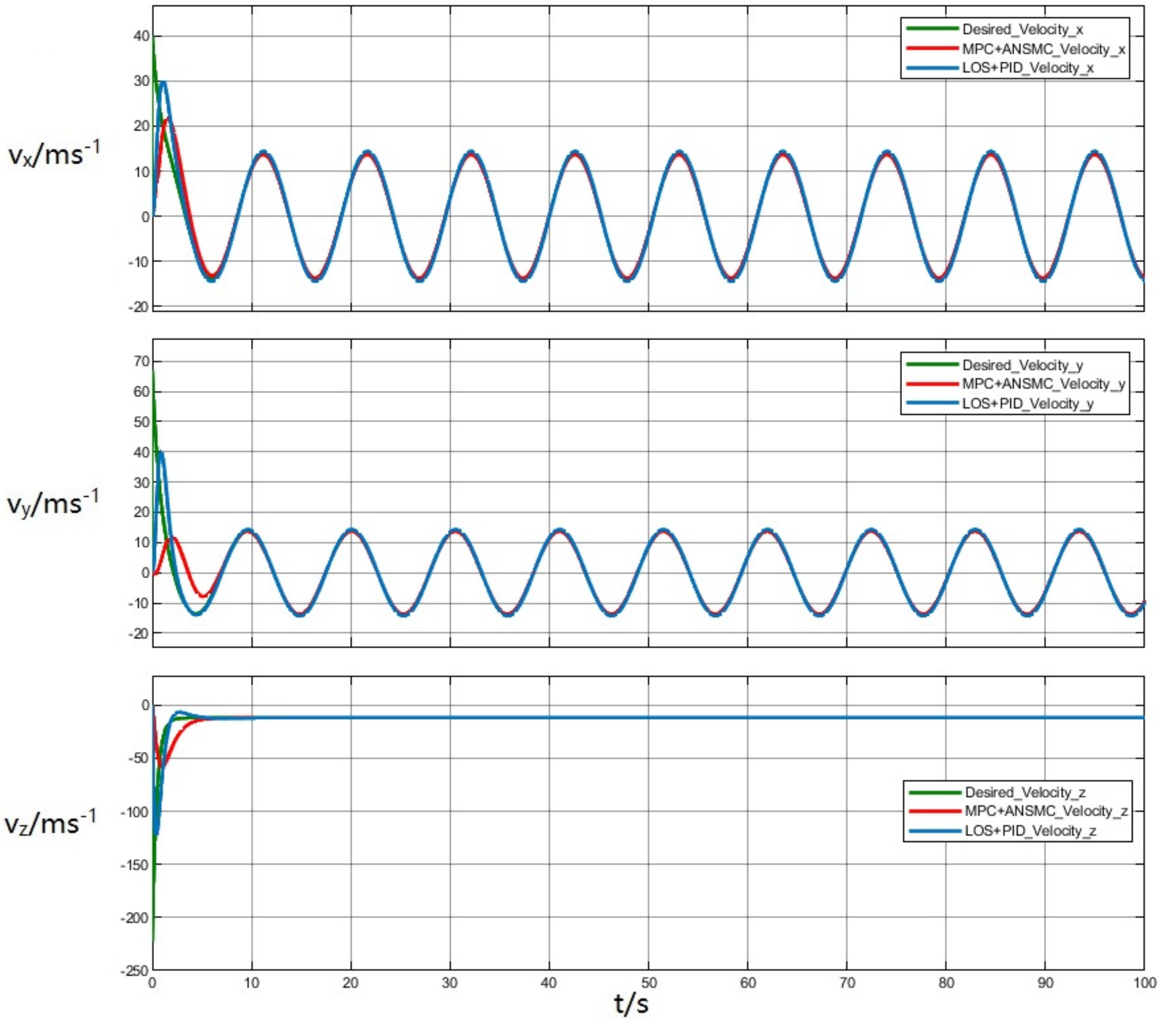

Fig 8. The velocity variations of the tiltrotor UAV

In the figure, the green curve represents the reference velocity obtained by processing the input target trajectory, which is defined in the geodetic coordinate system {G}. The red curve shows the actual velocity changes of the tiltrotor UAV when performing the trajectory tracking task under the controller designed in this paper. The blue curve indicates the velocity changes of the tiltrotor UAV when executing the trajectory tracking task under a controller with a LOS+PID control strategy. It can be observed that the controller designed in this paper enables the tiltrotor UAV to complete the task with a smoother response compared to the traditional LOS+PID controller.

Variations in the magnitude of position errors for tilt-rotor unmanned aerial vehicles during trajectory tracking tasks within the geodetic coordinate system {G}:

In the figure presented, the red curve illustrates the error between the actual path and the target trajectory of the tiltrotor UAV when tracking the trajectory using the controller designed in this study. The blue curve depicts the error in the trajectory tracking task of the tiltrotor UAV when employing a controller with a LOS+PID control strategy. It is evident that compared to the conventional LOS+PID controller, the controller proposed in this paper significantly reduces the tracking error of the tiltrotor UAV.

The simulation results indicate that, in the task of following a helical path, the controller designed in this study exhibits advantages over the controller with a LOS+PID control strategy, including reduced overshoot and faster convergence. Consequently, it can be inferred that the proposed controller demonstrates superior performance in tracking common curvilinear reference paths in three-dimensional space.

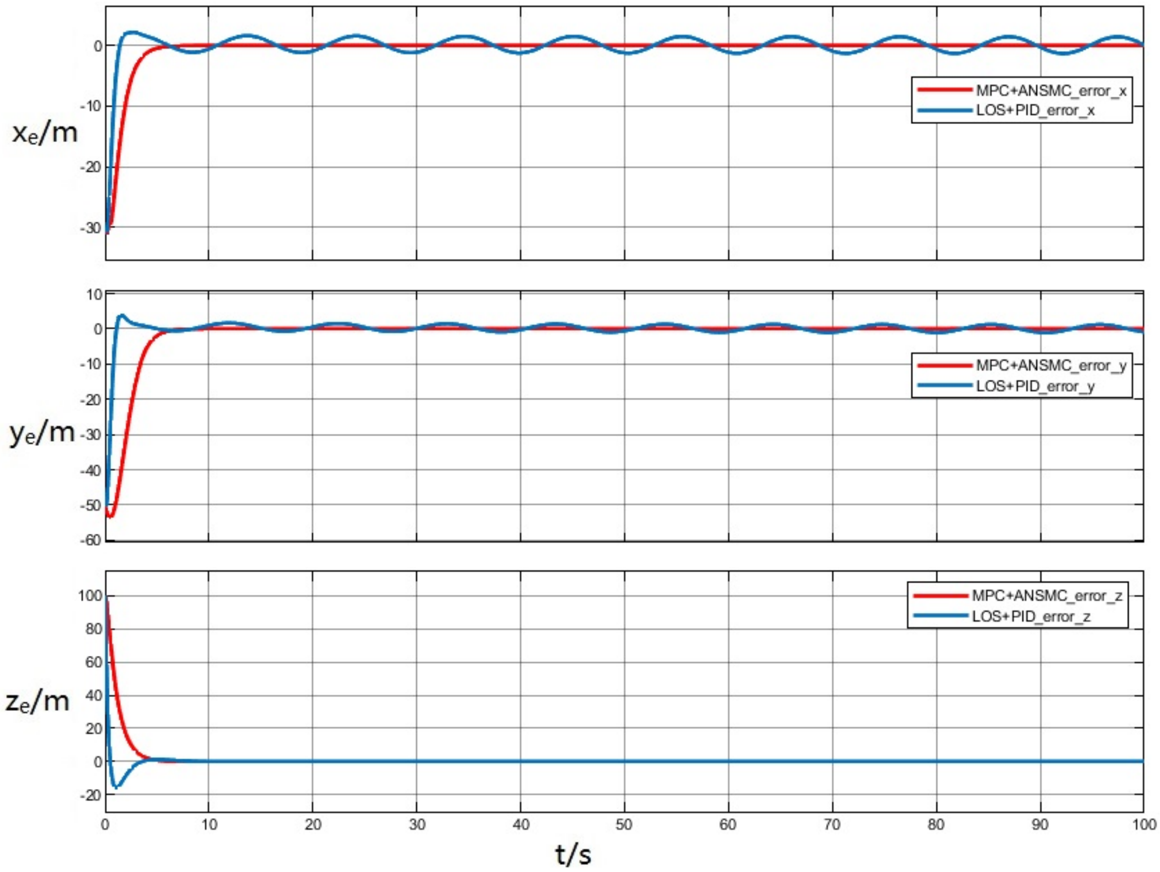

Fig 9. The positional errors of the tiltrotor UAV

5. Conclusion

This paper presents the kinematic and dynamic modeling for the tiltrotor UAV. Based on the established models, a control strategy for the tiltrotor UAV, which integrates Model Predictive Control (MPC) and Adaptive Sliding Mode Control (ASMC), has been implemented. The controller is designed utilizing a model established on the basis of path tracking errors, and it meticulously controls both kinematics and dynamics, enabling precise tracking of various flight paths. Furthermore, extensive simulation experiments were conducted to test waypoint tracking, straight-line path tracking, spiral path tracking, and wave path tracking.

In comparative simulation experiments, the designed controller was benchmarked against a controller employing a Line-Of-Sight (LOS) plus Proportional-Integral-Derivative (PID) control strategy. The experimental results demonstrate the significant superiority of our tiltrotor UAV control strategy, which leverages MPC and sliding mode control, in terms of both flight path tracking precision and stability, outperforming the LOS+PID control strategy.

The research work in this chapter not only enhances the stability and precision of tiltrotor UAV flying in complex environments but also showcases the considerable potential of Model Predictive Control and Sliding Mode Control in practical applications. These research findings lay an important foundation for the design and optimization of UAV flight control strategies in the future.

References

[1] Hoffmann G M, Waslander S L, Tomlin C J. Quadrotor helicopter trajectory tracking control[C]//AIAA guidance, navigation and control conference and exhibit. 2008: 1-14.

[2] Bouktir Y, Haddad M, Chettibi T. Trajectory planning for a quadrotorhelicopter [C]//Control and Automation, 2008 16th Mediterranean Conference on. IEEE, 2008: 1258-1263.

[3] Chamseddine A, Zhang Y, Rabbath C A, et al. Flatness-based trajectory planning/replanning for a quadrotor unmanned aerial vehicle [J]. Aerospace and Electronic Systems, IEEE Transactions on, 2012, 48(4): 2832-2848.

[4] Mofid O, Mobayen S, Zhang C W, et al. Desired tracking of delayed quadrotor UAV under model uncertainty and wind disturbance using adaptive super-twisting terminal sliding mode control[J]. ISA Transactions, 2022, 123: 455-471.

[5] M.R. Mortazavi, A. Naghash , Pitch and flight path controller design for f-16 aircraft using combination of LQR and EA techniques, Proc. IMechE Part G 232 (10) (2018) 1831–1843 .

[6] Silvestre C, Pascoal A, Kaminer I (2002) On the design of gainscheduled trajectory tracking controllers. Int J Robust Nonlinear Control 12(9):797–839.

[7] Antonelli G, Caccavale F, Chiaverini S, Fusco G (2003) A novel adaptive control law for underwater vehicles. IEEE Trans Control Syst Technol 11(2):221–232.

[8] Li JH, Lee PM (2005) Design of an adaptive nonlinear controller for depth control of an autonomous underwater vehicle. Ocean Eng 32(17–18):2165–2181.

[9] Zhang LJ, Qi X, Pang YJ (2009) Adaptive output feedback control based on DRFNN for AUV. Ocean Eng 36(9):716–722.

[10] Fossen TI, Lekkas AM (2017) Direct and indirect adaptive integral line-of-sight path-following controllers for marine

craft exposed to ocean currents. Int J Adapt Control Signal Process 31(4):445–463.

[11] Ji DX, Liu J, Zhao HY, Wang YQ (2014) Path following of autonomous vehicle in 2D space using multivariable sliding mode control. J Robot 2014:1–6.

[12] Xu J, Wang M, Qiao L (2015) Dynamical sliding mode control for the trajectory tracking of underactuated unmanned underwater vehicles. Ocean Eng 105:54–63.

[13] Pan CZ, Lai XZ, Yang SX, Wu M (2015) A bioinspired neural dynamics-based approach to tracking control of autonomous surface vehicles subject to unknown ocean currents. Neural Comput Appl 26(8):1929–1938.

[14] Yao XL, Yang GY, Peng Y (2017) Nonlinear reduced-order observer-based predictive control for diving of an autonomous underwater vehicle. Discrete Dyn Nat Soc 2017:1–15.